Pecking Mechanism inspired by Avian Cranial Kinesis for Flapping Wing Aerial Manipulators

Saad Hussain, Abner Asignacion Jr. and Satoshi Suzuki* Chiba University, Japan

ABSTRACT

This study introduces a new manipulation system for Flapping Wing MAVs (FW-MAVs) based on avian beak movements. The design draws inspiration from avian Cranial Kinesisthe bone movement mechanism in bird skulls to create a lightweight grasping/pecking mechanism for FW-MAVs. In bird anatomy, coordinated muscle actions drive skull bone movements, enabling complex tasks like pecking and grasping. The proposed design simplifies this biological system into a single-degree-of-freedom mechanism suitable for lightweight FW-MAVs. Key features of bird skull anatomy are adapted through simplified bone structures and a flexible neck to replicate natural movements. The resulting mechanism achieves wide beak opening and strong gripping force while maintaining a minimal weight of 15.3 g. Static and flight tests evaluated system performance across multiple tasks: object transport, leaf manipulation, plant sample collection, and suspended target interaction. All tasks were successfully completed with maintained flight stability.

1 Introduction

The field of micro air vehicles (MAVs) has experienced significant expansion, with applications emerging in surveillance, search and rescue operations, and structural inspections. Conventional MAVs utilize high-speed propellers, which present safety concerns in close-quarter operations. An alternative approach based on flapping wing MAVs (FW-MAVs) addresses these limitations through bio-inspired wing movements. The resulting systems exhibit reduced noise levels and increased efficiency, particularly in confined spaces and sensitive environments. Despite these advantages and inherent mechanical resilience, the challenge of enabling physical environmental interaction in FW-MAVs remains to be addressed.

To address this challenge and leverage these characteristics, researchers have developed bio-inspired perching systems based on avian and insect behavior[1, 2, 3]. Such systems enable FW-MAVs to attach to various surfaces and objects, facilitating inspection and data collection tasks while

*Email address: suzuki-s@chiba-u.jp

minimizing energy consumption compared to sustained hovering. However, current designs are limited to perching functionality and lack capabilities for more complex interactions such as pecking, grasping, pulling, or pushing. Despite the potential advantages FW-MAVs hold over conventional MAVs for sample collection and manipulation tasks, research on systems enabling these advanced interactions remains limited and largely impractical.

Consider, for instance, existing dual-arm manipulators designed for ornithopters [4, 5, 6]. These systems combine six servo motors and two scissor-equipped arms, but their 100 g weight restricts their use to only large-scale FWUAVs. Their rigid design also makes quick, reliable movements challenging. Similarly, while perching grippers for conventional multirotor UAVs [7] can effectively grasp and pull objects, they lack the ability to perform pushing or pecking actions. Therefore, a new approach to interact with the environment is necessary to enable advanced aerial manipulation with FW-MAVs.

Avian beak systems provide remarkable environmental interaction capabilities through specialized mechanisms. The integration of beak structures with flexible neck movements enables tasks ranging from precise manipulation to forceful interactions. Species-specific adaptations can be observed: falcons and hummingbirds demonstrate aerial precision in prey capture and nectar feeding, while woodpeckers and sparrows exhibit powerful pecking abilities in foraging and nest construction. These functions arise from two key anatomical features: the flexible neck system and a specialized bone movement mechanism known as Cranial Kinesis.

The skull movement mechanism operates through coordinated jaw muscle activation for bone movement control. This biological system achieves operational efficiency through a combination of wide beak opening and precise positional control, facilitating both forceful and delicate object manipulation.

Analysis of avian Cranial Kinesis biomechanics reveals key principles in bone configuration, joint structure, and muscle arrangement, enabling the development of lightweight and effective mechanisms for aerial manipulation in FW-MAVs. Although the avian skull comprises multiple muscles and bones, prior studies [8, 9] have demonstrated the possibility of expressing essential beak movement as a single degree of freedom (1-DoF) mechanism. Such simplification provides an ideal model for ultra-light manipulator design in lightweight FW-MAVs. The integration of this bio-inspired

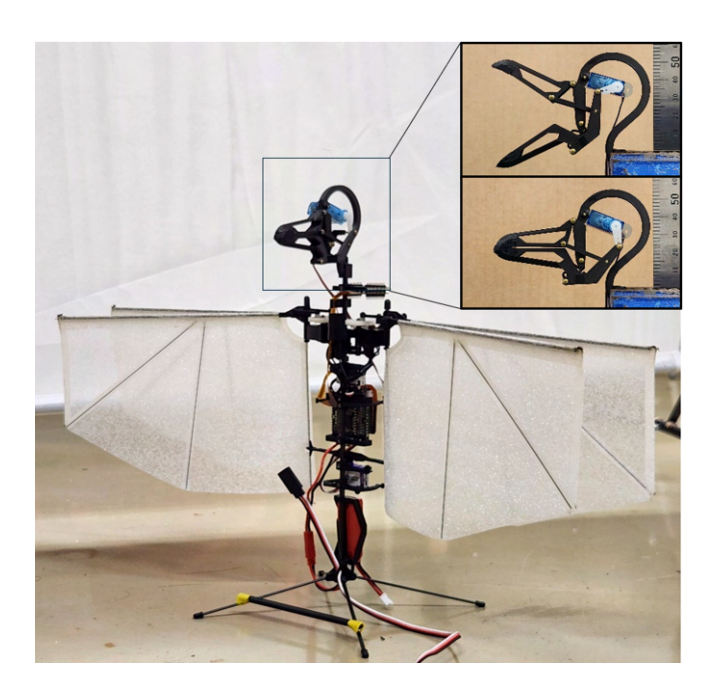


Figure 1: Pecking mechanism mounted on the Nimble+

mechanism with existing perching systems enables advanced manipulation capabilities such as pecking, grasping, pulling and pushing, thus expanding FW-MAV functionality beyond basic environmental interaction.

These biomechanical insights informed the development of a novel pecking mechanism that integrates avian Cranial Kinesis principles with a compliant neck design, replicating essential beak movements while providing impact resilience. Section 2 presents the mechanism details, followed by performance evaluation tests in Section 3. The paper concludes with Section 4.

2 DESIGN

Drawing from avian Cranial Kinesis principles, this study presents a pecking mechanism with kinematic architecture analogous to the avian skull structure, incorporating a passively compliant neck for impact absorption. The experimental platform utilizes the Nimble+ system from *Flapper Drones*, an X-shaped FW-MAV selected for its suitable configuration. Table 1 shows the specifications of the Nimble+ platform, while Figure 1 illustrates the integration of the mechanism with the airframe. A detailed analysis of the mechanism's architecture and operation follows in Section 2.2.

2.1 Avian Cranial Kinesis

To create an effective and lightweight pecking mechanism, we began by studying how birds move their beaks. Research has identified three main types of skull movement in vertebrates with hinged upper jaws [8, 9]. These types are named based on where the hinge connects the upper beak to the skull: metakinesis (hinge at the skull's rear), mesokinesis

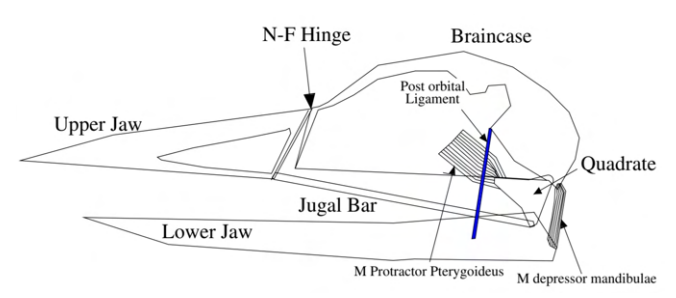


Figure 2: The mechanism of Avian Cranial Kinesis [9]

(hinge between the forehead and crown bones), and prokinesis (hinge between the nose and forehead bones). Birds typically use prokinetic skull movement, which allows them to open their beaks extremely wide. This wide opening is crucial for feeding, as it creates a large target area and makes it easier to catch or grasp objects.

As described in [9] and shown in Figure 2, a bird's skull uses five key bones to move its beak: (1) the upper jaw, (2) a connecting rod called the jugal bar, (3) the lower jaw, (4) a pivot bone called the quadrate, and (5) the braincase. The braincase stays fixed and connects to the upper jaw through a flexible hinge called the nasal-frontal (N-F) hinge. When muscles move the quadrate bone back and forth, the jugal bar transfers this motion to raise and lower the upper jaw. This efficient design works because muscles only need to move the quadrate and lower jaw, while the braincase provides a stable anchor point.

In prokinesis, the most common form of Cranial Kinesis in birds, forward movement of the quadrate bone initiates a coordinated motion sequence: the jugal bar is displaced anteriorly, elevating the upper jaw, while simultaneously the lower jaw rotates ventrally around the post-orbital ligament's terminus, creating a wide gape. The reverse motion occurs when the quadrate shifts posteriorly—the jugal bar draws the upper jaw downward while the lower jaw executes a clockwise rotation about the same pivot point, closing the beak.

This biomechanical system demonstrates remarkable efficiency: despite the involvement of multiple muscles in avian Cranial Kinesis, the fundamental jaw movement can be reduced to the singular motion of the quadrate bone. This mechanical simplification enables the entire system to be mod-

Weight (Without Shell)	102 g
Payload	25 g
Height	25 cm
Wingspan	49 cm
Battery	LiPo 2S 300 mAh
Flight time (with 25 g payload)	5 min

Table 1: Specifications of Nimble+ by Flapper Drones

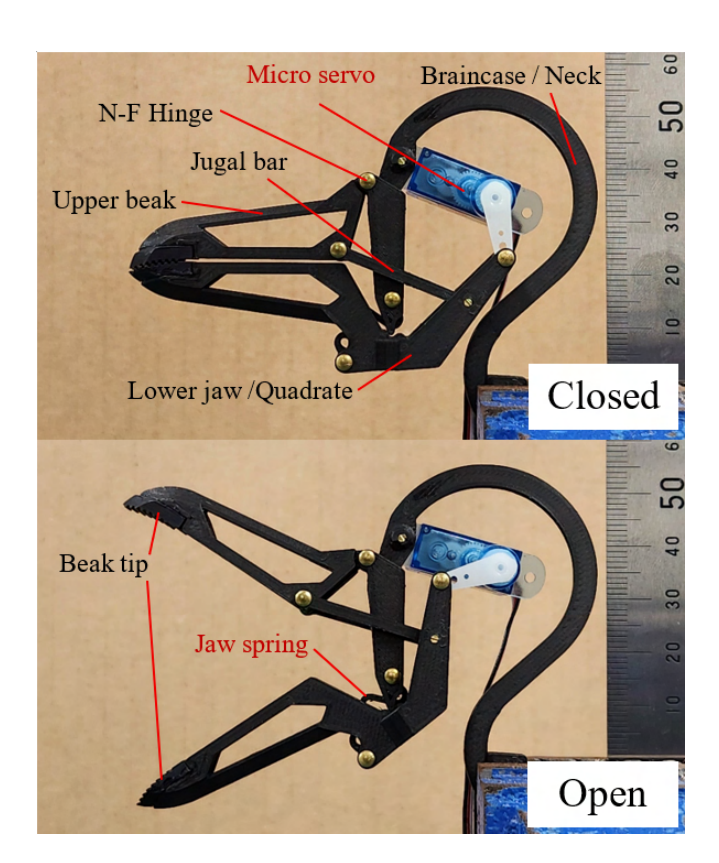


Figure 3: The proposed grasping/pecking mechanism

eled as a single-degree-of-freedom (1-DoF) mechanism.

2.2 Mechanism

As outlined in Section 2.1, birds achieve beak movement through a system where muscles connect to two key components: the quadrate bone and lower jaw. The quadrate serves as the primary driver, rotating around a fixed point in the skull to create the desired motion.

Our study of beak movements in common birds revealed two key observations:

- The quadrate bone and lower jaw rotate around points that are very close together
- The post orbital ligament shows minimal pivoting motion

These anatomical characteristics enabled significant design simplification. The post orbital ligament functions effectively as an extension of the fixed braincase structure, allowing the integration of the quadrate and lower jaw into a single L-shaped component. This unified structure rotates around the original post orbital ligament connection point at the braincase tip.

Based on these simplifications, the avian Cranial Kinesis mechanism can be reduced to fewer components while maintaining functional equivalence. Applying these principles, a lightweight grasping/pecking mechanism was devel-

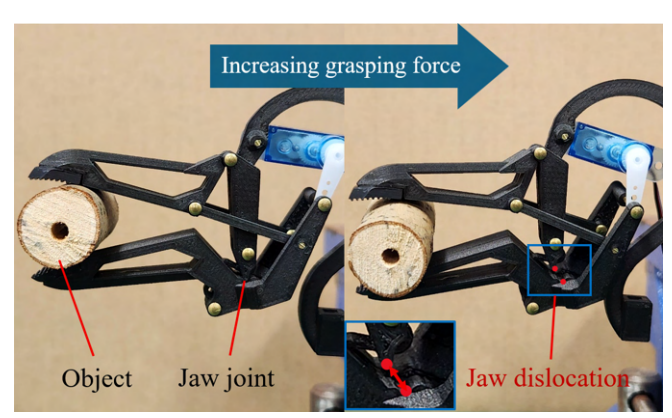


Figure 4: Dislocation of the jaw joint

oped that replicates the essential kinematic behavior of avian Cranial Kinesis with minimal structural complexity. The implemented design is illustrated in Figure 3.

The proposed design consists of five key components: the upper beak, a combined lower jaw-quadrate element, a motion-transferring jugal bar, a braincase-neck structure, and a servo motor system. Jaw movement is driven by a compact 4.9 g servo motor, including wiring, through rotation at the jaw joint. The resulting rotation is transferred through the jugal bar to control upper beak position. Grooved surfaces are incorporated into the beak tips to enhance grip strength during object manipulation.

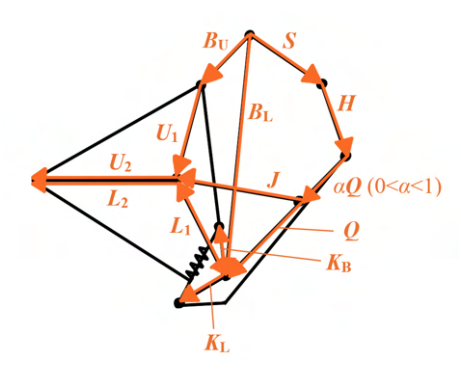
The implemented 1-DoF mechanism achieves a minimal mass of 15.3 g and is designed for dorsal mounting on the FW-MAV platform, analogous to avian head positioning. The integration configuration is illustrated in Figure 1.

Complementing the simplified kinematic structure, the mechanism incorporates two key features for enhanced operational robustness: a compliant neck interface and an impact-mitigation system. The compliant neck structure provides a flexible coupling between the mechanism and the FW-MAV airframe, facilitating impact absorption during environmental interactions. Additionally, the mechanism features a spring-loaded dislocatable jaw joint, engineered to provide controlled mechanical compliance during high-force interactions.

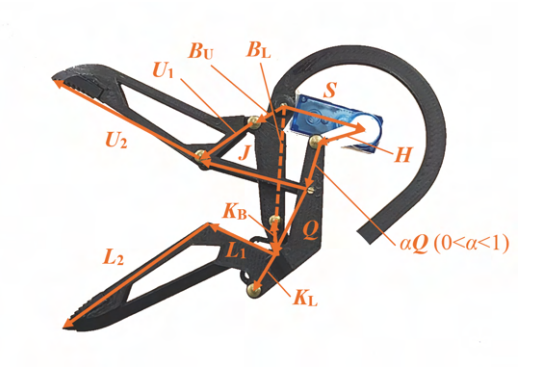
During high-force interactions, the design incorporates controlled jaw dislocation. This feature allows the integrated spring to absorb excess energy and modulate the applied force, thereby protecting the structural integrity of the system. Figure 4 illustrates this adaptive behavior during the grasping of a round object.

2.3 Link Model

A simplified link model was developed to mathematically describe the mechanism's kinematics. Figure 5 presents the link-based structure, while Figure 6 illustrates the corresponding joint configurations, including initial angles (a) and variable angles (b). The mathematical formulation enables



(a) Vector parameters of the link model



(b) Vector parameters showed on the mechanism

Figure 5: Link model: vector parameters

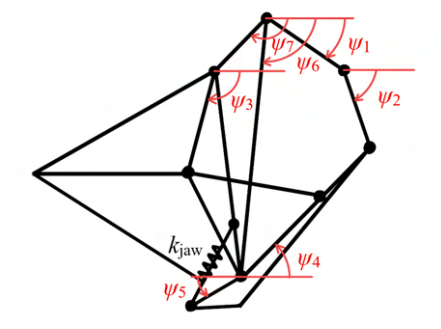
prediction of beak opening width and operational angles.

The norms of the vectors in Figure 5, representing the physical link lengths, are denoted by the same letters as their corresponding vectors (e.g., S represents the magnitude of vector S). In Figure 6, angles are denoted by ψ and ϕ , where ψ represents the initial fixed angles and ϕ denotes the variable joint angles during operation. The input angle θ corresponds to the servo motor rotation angle.

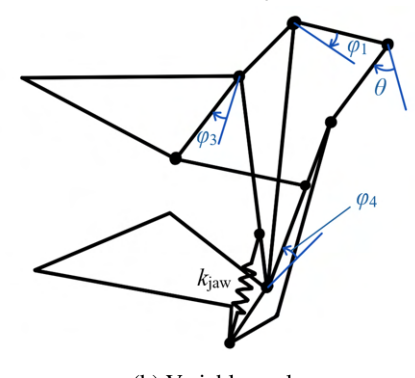
The mechanism's operation begins with the rotation of input vector \boldsymbol{H} about the terminus of vector \boldsymbol{S} . This rotation actuates the quadrate portion of the lower jaw \boldsymbol{Q} , inducing rotation about the jaw joint. Simultaneously, this motion drives the jugal bar \boldsymbol{J} , which actuates the upper beak $\boldsymbol{U_2}$ through rotation about the N-F hinge $\boldsymbol{B_U}$, resulting in jaw opening. During this sequence, the jaw spring link $\boldsymbol{K_L}$ undergoes rotation, extending the jaw spring k_{jaw} and storing potential energy for subsequent grasping operations.

Now that the link model is defined, mathematical relationships describing the beak movements can be developed. These equations will help determining the beak's opening width and angle during operation. For consistency in following calculations, the \boldsymbol{S} is set as a reference point (origin).

Using the upper beak vector $oldsymbol{U_2}$ and the lower jaw vector



(a) Initial angles



(b) Variable angles

Figure 6: Link model: angle parameters

 L_2 , the beak tip position vectors can be expressed as:

$$U = B_U + U_1 + U_2 \tag{1}$$

$$L = B_L + L_1 + L_2 \tag{2}$$

Here, U and L are the upper and lower beak tip position vectors, respectively. A detailed formulation can be obtained from the lengths and angles of the links.

$$\begin{bmatrix} U_x \\ U_y \end{bmatrix} = \begin{bmatrix} -B_U \cos \psi_7 + U_1 \cos(\psi_3 + \phi_3) - U_2 \cos \phi_3 \\ B_U \sin \psi_7 + U_1 \sin(\psi_3 + \phi_3) - U_2 \sin \phi_3 \end{bmatrix}$$
(3)

$$\begin{bmatrix} L_x \\ L_y \end{bmatrix} = \begin{bmatrix} -B_L \cos \psi_6 + L_1 \cos(\psi_4 + \phi_4) - L_2 \cos \phi_4 \\ B_L \sin \psi_6 + L_1 \sin(\psi_4 + \phi_4) - L_2 \sin \phi_4 \end{bmatrix}$$
(4)

Beak tip opening distance is given by the vertical component of the difference between the upper and lower beak tip position vectors. By substituting equation 3 and equation 4, the beak tip opening distance d_{tip} can be expressed as:

$$d_{tip} = |\mathbf{U} - \mathbf{L}|_{y}$$

$$= B_{U} \sin \psi_{7} + U_{1} \sin(\psi_{3} + \phi_{3}) - U_{2} \sin \phi_{3}$$

$$- [B_{L} \sin \psi_{6} + L_{1} \sin(\psi_{4} + \phi_{4}) - L_{2} \sin \phi_{4}] \quad (5)$$

The same can be done for the beak root opening distance

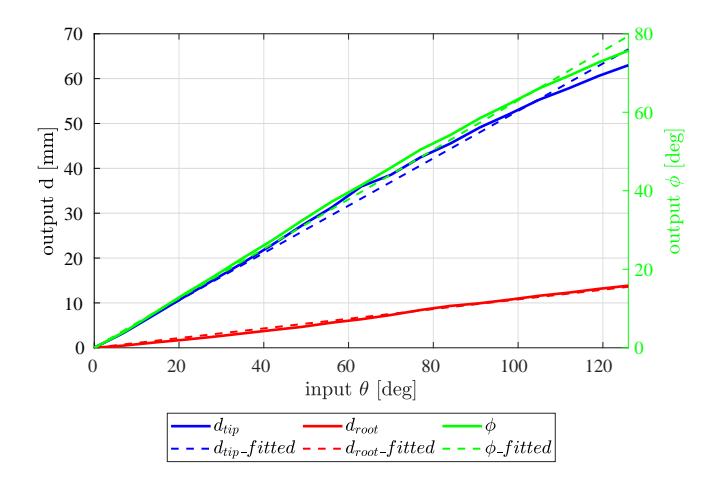


Figure 7: Measured and fitted outputs of the mechanism

 d_{root} .

$$d_{root} = |(U - U_2) - (L - L_2)|_y$$

= $B_U \sin \psi_7 + U_1 \sin(\psi_3 + \phi_3)$
- $[B_L \sin \psi_6 + L_1 \sin(\psi_4 + \phi_4)]$ (6)

The beak opening angle ϕ is the angle between the upper and lower beaks, and can be expressed as:

$$\phi = \phi_3 + \phi_4 \tag{7}$$

As a single-degree-of-freedom mechanism, the key outputs d_{tip} , d_{root} , and ϕ depend solely on the input angle θ . By determining the relationships between joint angles and the input θ , we can precisely control these outputs through servo motor positioning. The mechanism's design allows for adjustment of link parameters to achieve different beak opening ranges and angles, enabling adaptation for various UAV platforms and applications. Table 2 lists the parametric values used in our implementation.

To simplify the output equations, a CAD model of the mechanism was used to measure the outputs of different input angles. The resulting discrete data were plotted, and linear fitting was applied to approximate the corresponding equations. The plotted data and the fitted equations are shown in figure 7. The equations are expressed as below.

$$d_{tip} = 0.5280 * \theta \quad [mm] \tag{8}$$

$$d_{root} = 0.1079 * \theta \quad [mm] \tag{9}$$

$$\phi = 0.5630 * \theta \quad [deg] \tag{10}$$

3 EXPERIMENTS AND EVALUATION

The pecking mechanism evaluation consisted of two main testing phases: static force analysis and dynamic flight trials. Static testing measured gripping capabilities across objects of various materials and sizes. Dynamic flight trials evaluated four key manipulation tasks: payload transport, grasping



Figure 8: Sample objects for static grasping experiment

and pulling operations, sample collection, and pecking maneuvers. The experimental methodology focused on mechanism performance assessment under realistic operating conditions.

3.1 Grasping Force Test

Force measurements using a Newton meter were conducted to quantify gripping capabilities across six test specimens of varying materials and dimensions. The experimental protocol involved rope attachment to specimens, Newton meter coupling, and progressive tension application until grip failure occurred. Video documentation of force readings enabled peak value determination for maximum grip strength analysis. The experiment was performed 3 times for all objects. The objects are shown in Figure 8, and the experiments were conducted as shown in Figure 9. The objects are all cylindrical, and are categorized in 2 sizes and 3 materials. The sizes are 12 mm and 18 mm, and the materials are smooth branch (left), rough branch (center), and soft TPU (right).

The results are shown in Figure 10. In this box-and-whisker plot, the vertical axis represents the maximum gripping force. For each object, the plot shows the range and the mean-maximum gripping force. The mean value is indicated by the black line inside the boxes.

The mean-maximum grasping force was the highest for the 18 mm rough branch at 3.03 N, followed by 2.29 N for the 18 mm soft TPU, 2.06 N for the 12 mm soft TPU, 1.63 N for the 12 mm rough branch, 0.96 N for the 18 mm smooth branch, and lastly 0.93 N for the 12 mm smooth branch.

The results show that larger objects (18 mm diameter)

Length [mm]			Angle [deg]		
\overline{S}	18.8	U_2	40.0	ψ_1	19.1
H	11.5	L_1	16.0	ψ_2	83.0
Q	15.0	L_2	40.0	ψ_3	111.6
J	25.3	K_B	6.0	ψ_4	24.7
B_L	31.9	K_L	10.0	ψ_5	30.0
B_U	7.6	α	0.7 [-]	ψ_6	92.4
U_1	13.9			ψ_7	147.1

Table 2: Mechanism parametric values

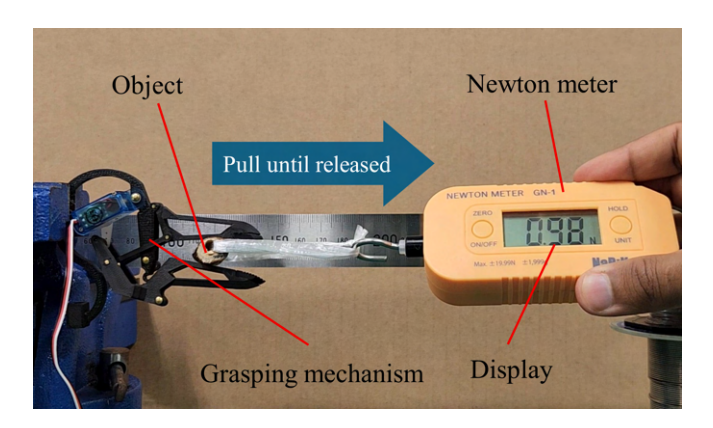


Figure 9: Static grasping experiment

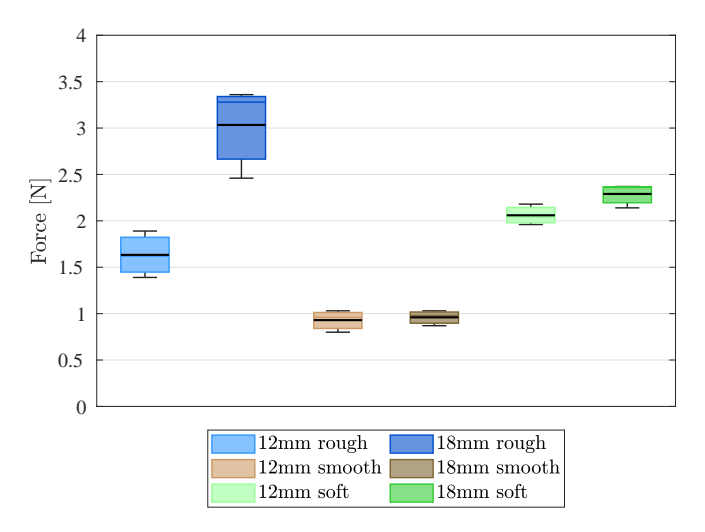


Figure 10: Static grasping experiment result

consistently required more force to dislodge than smaller ones across all materials tested. This difference was most pronounced with the rough branch, moderate with the soft TPU, and minimal with the smooth branch. The increased grip strength on larger objects can be attributed to their greater contact area with the beak surfaces. When gripped, the objects experience slight deformation at the contact points. Larger objects, having more gradual curves, create wider contact areas under the same gripping pressure, leading to stronger overall grip force. This relationship explains the minimal force differential observed with the smooth branch, as its rigid structure resists deformation under the mechanism's grasping force. Notably, the force difference between size variants is greater for the rough branch than for the soft TPU, despite TPU's higher compressibility. This unexpected result stems from surface characteristics: the rough wood's surface protrusions interact mechanically with the grooved beak tips, enhancing grip through physical interlocking rather than material deformation alone.

Analysis of force measurement variability reveals that smooth-surfaced objects (smooth branch and soft TPU) ex-



Figure 11: Piece of a plant as a payload (6.7 g)

hibited 60% less variation in maximum grasping force compared to the rough branch. While rough surfaces generated higher peak grip forces, smooth surfaces demonstrated superior consistency in force application, suggesting enhanced operational reliability and repeatability.

The minimum measured grasping force of 0.93 N exceeded the mechanism's weight by a factor of 5.96, demonstrating robust gripping capability across the full range of test specimens, independent of material properties, surface characteristics, and geometric variations.

3.2 Flight Experiments

Following validation of the mechanism's static grasping capabilities across diverse object types, dynamic flight testing was conducted to evaluate performance in realistic operational scenarios. Four distinct manipulation tasks were executed to assess aerial manipulation capabilities. The experimental platform incorporated a nonlinear disturbance observer-based robust controller [10]. Mounted on the Nimble+ platform (figure 1), the mechanism responded to external control inputs throughout the aerial manipulation sequences.

3.2.1 Payload Transportation Task

In this experiment, the capability to successfully carry a payload to a different location while flying was tested through a payload transportation task. First, the payload shown in Figure 11 is placed to be grasped by the mechanism. After that, the drone starts by hovering, and then transitions to start maneuvering around, demonstrating carrying a payload to a different location. The flight experiment is shown in Figure 12.

Here, the mechanism's ability to transport payloads during flight was tested using the sample shown in Figure 11. The test sequence began with positioning the payload for grasping. Once secured, the MAV took off into a stable hover before executing a series of maneuvers to demonstrate payload transport capability. Figure 12 shows the key stages of this flight experiment.

The experiment demonstrated stable payload transport throughout the flight sequence, with the mechanism maintaining a secure grip while the MAV performed various maneuvers. These results confirm the design's practical utility for aerial payload transport applications.

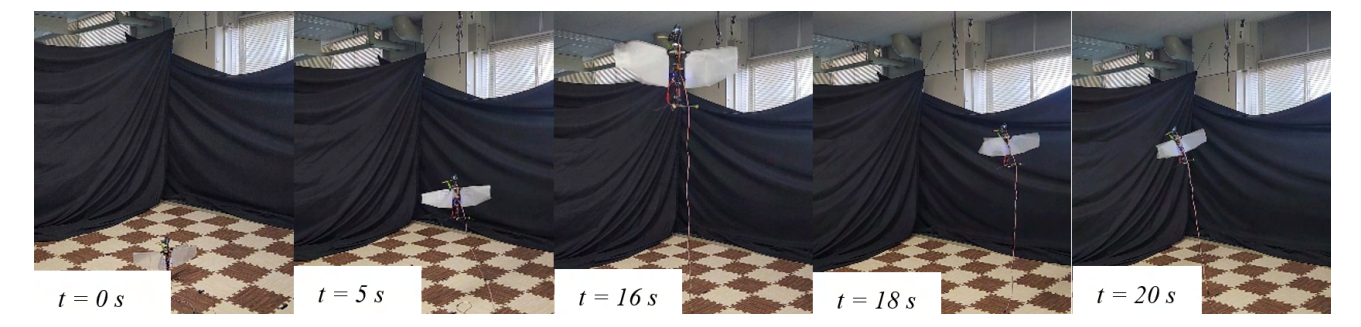


Figure 12: Payload Transportation task



Figure 13: Grasping and Pulling task

3.2.2 Grasping and Pulling Task

To simulate real-world tasks, system's ability to grasp and manipulate objects before transportation was tested. For this evaluation, a potted plant was positioned at a set distance from the takeoff point. After takeoff, the MAV approached the plant in a controlled manner. When positioned near the target leaf, the beak mechanism was opened. The MAV then moved closer for precise positioning, allowing the beaks to close and secure the leaf. Once grasped, the MAV tested the grip strength by pulling in different directions. The flight experiment is shown in Figure 13.

The approach maneuver execution resulted in successful leaf acquisition. Multi-directional loading tests demonstrated stable grip integrity, with maintained hold observed under maximum thrust conditions. These results validate system capabilities for manipulation tasks requiring sustained force application.

3.2.3 Grasping and Sample Collection Task

The complete sample collection sequence consisted of approach, grasp, detach, and transport operations. The experimental methodology followed procedures outlined in Section 3.2.2, targeting branch sample retrieval and return to the initial position. Double-sided tape secured the test specimen to an existing branch. Figure 14 documents the complete flight sequence.

The experiment demonstrated successful sample retrieval and landing operations. The demonstrated collection capabilities, while successful in controlled conditions, indicate the necessity for an integrated cutting mechanism in practical field applications for direct vegetation sampling.

3.2.4 Pecking Task

The final experimental phase evaluated forward force application capabilities through pecking motions. The test setup employed a suspended banana as the target object. Experimental procedures consisted of target approach followed by pecking motion execution. Results demonstrated flexible neck effectiveness in impact force absorption and primary structure protection.

The impact force proved sufficient for target displacement, while the neck's compliance characteristics enabled stable flight maintenance throughout the impact sequence.

4 CONCLUSION

A bio-inspired aerial manipulation system based on avian Cranial Kinesis principles is introduced in this study. The proposed single-degree-of-freedom design replicates key skeletal movements of bird skulls, achieving substantial beak articulation and grip force while maintaining minimal mass. Through static force analysis and dynamic flight trials, successful execution of diverse manipulation tasks was demonstrated, including object transport, grip-and-pull operations,



Figure 14: Grasping and Sample Collection task

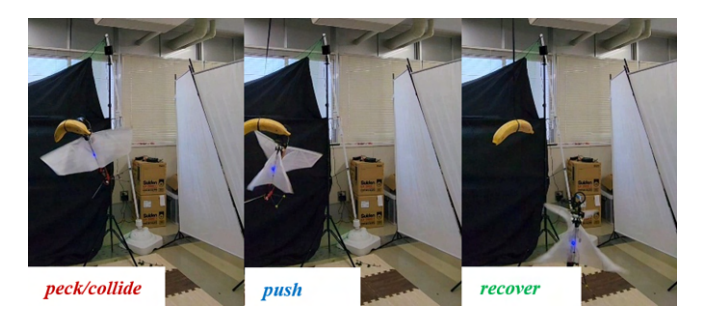


Figure 15: Pecking task

and pecking maneuvers. Future development directions include design optimization, integration of cutting functionality within the current kinematic framework, and implementation of advanced control architectures for enhanced operational capabilities.

ACKNOWLEDGEMENTS

This work was supported by JSPS KAKENHI Grant Number JP23K13274 (Grant-in-Aid for Early-Career Scientists)

REFERENCES

- [1] Raphael Zufferey, Jesus Tormo-Barbero, D. Feliu-Talegón, et al. How ornithopters can perch autonomously on a branch. *Nature Communications*, 13(7713), 2022.
- [2] Ahmad Hammad, Mehmet Süer, and Sophie F. Armanini. A lightweight bioinspired sma-based grasping mechanism for flapping wing mavs. *Biomimetics*, 10(6), 2025.
- [3] Krispin Broers and Sophie Armanini. Repeatable energy-efficient perching for flapping-wing robots using soft grippers, 09 2024.
- [4] Saeed Rafee Nekoo, Daniel Feliu-Talegon, Raul Tapia, Alvaro C. Satue, Jose Ramiro Martínez-de Dios, and

- Anibal Ollero. A 94.1 g scissors-type dual-arm cooperative manipulator for plant sampling by an ornithopter using a vision detection system. *Robotica*, 41(10):3022–3039, 2023.
- [5] Rodrigo Gordillo Durán, Raul Tapia, Saeed Rafee Nekoo, José Ramiro Martínez-de Dios, and Anibal Ollero. Flapping-wing flying robot with integrated dual-arm scissors-type flora sampling system. In IEEE International Conference on Robotics and Automation (ICRA), 2025.
- [6] Sahar Sadeghi Kordkheili, Antonio Gonzalez-Morgado, Saeed Rafee Nekoo, Begoña C. Arrue, and Anibal Ollero. Optimal control of dual arm manipulation for flapping-wing robots in the post-perching phase. In 2025 International Conference on Unmanned Aircraft Systems (ICUAS), pages 155–161, 2025.
- [7] Krispin C. V. Broers and Sophie F. Armanini. Design and testing of a bioinspired lightweight perching mechanism for flapping-wing mavs using soft grippers. *IEEE Robotics and Automation Letters*, 7(3):7526–7533, 2022.
- [8] William Hoese and Mark Westneat. Biomechanics of cranial kinesis in birds: Testing linkage models in the white-throated sparrow (zonotrichia albicollis). *Journal of Morphology*, 227:305–320, 03 1996.
- [9] Preeda Meekangvan, Alan A. Barhorst, Thomas D. Burton, Sankar Chatterjee, and Lawrence Schovanec. Nonlinear dynamical model and response of avian cranial kinesis. *Journal of Theoretical Biology*, 240(1):32–47, 2006.
- [10] A. Asignacion S. Hussain, T. Matsuda and S. Suzuki. Nonlinear disturbance observer-based robust control for flapping-wing aerial manipulators. In *submitted to IEEE Trans of Mechatronics*, 2025. Under review.